Supporting Online Material for

Boron isotopic composition of olivine-hosted melt inclusions from Gorgona komatiites, Colombia: new evidence supporting wet komatiite origin

Andrey A. Gurenko[1,2]*, Vadim S. Kamenetsky[3]

[1] Woods Hole Oceanographic Institution, Geology & Geophysics, Woods Hole, MA 02543, USA

[2] Centre de Recherches Pétrographiques et Géochimiques, CNRS-Nancy Université, BP 20, F-54501 Vandoeuvre-lès-Nancy, France

[3] School of Earth Sciences and Centre for Ore Deposit Research, University of Tasmania, Australia

This file includes:

*** Corresponding author and present address:**

Andrey A. Gurenko, Centre de Recherches Pétrographiques et Géochimiques, 15, rue Notre-Dame des Pauvres, B.P. 20, 54501 Vandoeuvre-lès-Nancy, France.

Phone: +33 (0)3 83 59 48 75, Fax: +33 (0)3 83 51 17 98, E-mail: agurenko@crpg.cnrs-nancy.fr

S1. Analytical Methods

S1.1. High-temperature microthermometry of melt inclusions

Olivine phenocrysts containing melt inclusions (Fig. S1d-f) were wrapped in Pt foil together with a piece of graphite (to ensure reduced oxygen fugacity conditions), heated in a vertical furnace with a flow of pure Ar gas at 1275 °C for 2 min and, then, quenched in water (Kamenetsky et al., 2010). In order to determine more precisely the temperature of melt inclusion homogenization, a subset of olivine crystals with primary, regularly shaped melt inclusions were heated in the heating stage designed by Sobolev and Slutsky (1984) using visual control. After re-heating, the inclusions were transferred to brownish glass; a vapor bubble (<2 vol%), one or several sulfide globules, as well as occasionally trapped Cr-spinel crystal of variable size usually representing an inclusion nucleation center also may be present (Fig. S1f). The absence of tiny magnetite crystals in the heated melt inclusions (commonly seen as multiple black dots and originating due to hydrogen loss by diffusion during laboratory heating; Sobolev and Danyushevsky, 1994) rules out substantial water dissipation. The opposite process such as water gain described by Portnyagin et al. (2008) seems to be unlikely due to very low partial pressure of hydrogen in the gas mixture in either type of heating experiments. However, the presence of sulfide globules in some melt inclusions may point on the possible Fe loss in the included melts, occurred either during magma cooling in the lava flow or during experimental runs (Danyushevsky et al., 2002).

S1.2. Secondary Ion Mass Spectrometry

S1.2.1. Sample preparation

Olivine grains with homogenized melt inclusions were mounted in brass tubes 5 mm in diameter, ground and polished to expose melt inclusions and then placed in 1-inch round epoxy mounts. After curing the epoxy, the mounts were polished using Diamond Films of 3μm, 1 μm and 0.5 μm grain size and Glass Support Plates (ALLIED High Tech Products, Inc.) that minimizes the relief between the embedded olivine grains and enclosing epoxy resin (Kita et al., 2009). Prior gold coating, the mounts were ultrasonically cleaned in ethanol, then in de-ionized distilled H_2O and ultra pure H_2O and finally dried at 60–80 °C in the vacuum oven, following Chaussidon et al. (1997).

S1.2.2. Instrument setting

The $^{11}B/^{10}B$ ratios in homogenized melt inclusions were obtained using the CAMECA IMS 1280 ion microprobe at Woods Hole Oceanographic Institution, USA. The 13 kV $^{16}O^-$ primary beam of 15–20 nA current focused and then rastered to 30×30 um square was applied. Similar primary beam was used for sample pre-sputtering during 10 minutes before each run. A 400 μm contrast aperture and a 1000 μm field aperture were used, giving a field of view of approximately 25 μm. Secondary $^{10}B^+$ and $^{11}B^+$ ions were accelerated at 10 kV and analyzed at a mass resolving power ($M/\Delta M$) of ~2000, to resolve $^9Be^1H^+$ interference on $^{10}B^+$ peak and $^{10}B^1H^+$ interference on $^{11}B^+$ peak, using a circular focusing mode and a transfer optic of 150 μm. The energy slit was centered and opened to 50 V. The automatic routine of secondary beam centering in the field aperture was used at the beginning of each measurement. Typical ion intensities were 80–1200 cps of $^{10}B^+$ and 500–6000 cps of $^{11}B^+$ ions, depending primarily on B concentration in the glass. The 1 SD internal precision of individual measurements was ranging from 1.9 to 3.6‰ in the samples containing 0.6–2 μg/g B. The obtained precision was reached after 1–1.5 hours of counting (200–250 cycles, each including 10 and 5 seconds of counting time on the $^{10}B^+$ and $^{11}B^+$ peaks, respectively, and 2 seconds of waiting time between each mass

change). It matches well the Poisson counting statistics (1.9–3.5‰), implying that the instrument stability was maintained. After applying the correction of instrumental drift, the internal precision was improved to 1.4–2.6‰, giving in average 2.1‰.

S1.2.3. Instrumental mass fractionation and working curves

Rosner et al. (2008) have reported an analytical artifact related to the difference in instrumental mass fractionation between NIST SRM and natural standard glasses (in average +3.4‰). Because numerous factors related to instrument settings (e.g., setting of the primary and secondary ion optics, aging of the electron multiplier) may significantly affect instrumental mass fractionation values (IMF, expressed as a ratio of the measured to the true values, $\alpha_{IMF} = R_{measured}/R_{true}$), which may cause inter-laboratory bias, we carried out the detailed tests using our set of NIST SRM and natural reference glasses. This includes NIST SRM 610 and 612 standard glasses, multiple analyzed andesitic StHs6/80-G glass (11.6 µg/g B, δ^{11}B = –4.4‰; Rosner et al, 2008 and references therein), CRPG-CNRS internal reference GB4 glass resembling granodiorite (970 µg/g B, δ^{11}B = –12.9‰; Chaussidon and Jambon, 1994) and five basaltic reference glasses, GOR128-G (22.7 µg/g B, δ^{11}B = +13.6‰), GOR132-G (15.6 µg/g B, δ^{11}B = +7.1‰), ALV2746-15 (1.5 µg/g B, δ^{11}B = –7.1‰), ALV519-4-1 (0.32 µg/g B, δ^{11}B = –2.4‰) and CH7-1 (1.5 µg/g B, δ^{11}B = –10.3‰) (Jochum et al., 2000; Rosner and Meixner, 2004; Rosner et al., 2008; A. Shaw, personal communication, 2007).

As a result, we observe the average +3.3‰ offset of the NIST SRM glasses from the working curve based on the natural glasses at the instrument setting when α_{IMF} = 0.959 but only 0.7‰ difference was found at α_{IMF} = 0.971, as shown in Fig. S2. It is important to note that the analyses reported by Rosner et al. (2008) were acquired at α_{IMF} that was often lower than our values cited above (0.9197–0.9675). Given that no instrumental fractionation of isotopes is expected when ionization yield is 100% (i.e., α_{IMF} = 1), the experimentally measured α_{IMF} represents an "apparent ion yield" linked to the particular instrument setting. In other words, when the transmission of the instrument is optimized (that can be monitored achieving the highest α_{IMF} value) no effects described by Rosner et al. (2008) should be observed.

S1.2.4. Precision and accuracy

In order to infer the $^{11}B/^{10}B$ ratios in the unknown samples, we used exclusively IMF values obtained on the natural reference glasses GOR128-G, GOR132-G and StHs6/80-G. The δ^{11}B ratios were then calculated using $^{11}B/^{10}B$ = 4.04558 ± 0.00033 of the NBS 951 standard (Spivack and Edmond, 1986). One to three individual $^{11}B/^{10}B$ measurements were run on one or two selected reference glasses at the beginning and at the end of a data block (total number of measurements is 26 on StHs6/80-G, four on GOR128-G and three on GOR132-G), each including two to five unknown samples. The analytical error of a single B isotope measurement was thus defined, taking into account two sources of independent random errors: internal precision of the instrument (see above) and the uncertainty of IMF (i.e., its external reproducibility obtained during multiple measurements of standards) ranging from 0.3 to 0.8‰, 1 SE. This results in the uncertainty of δ^{11}B measurements, being in the range from 1.5 to 2.7‰ (average 2.2‰).

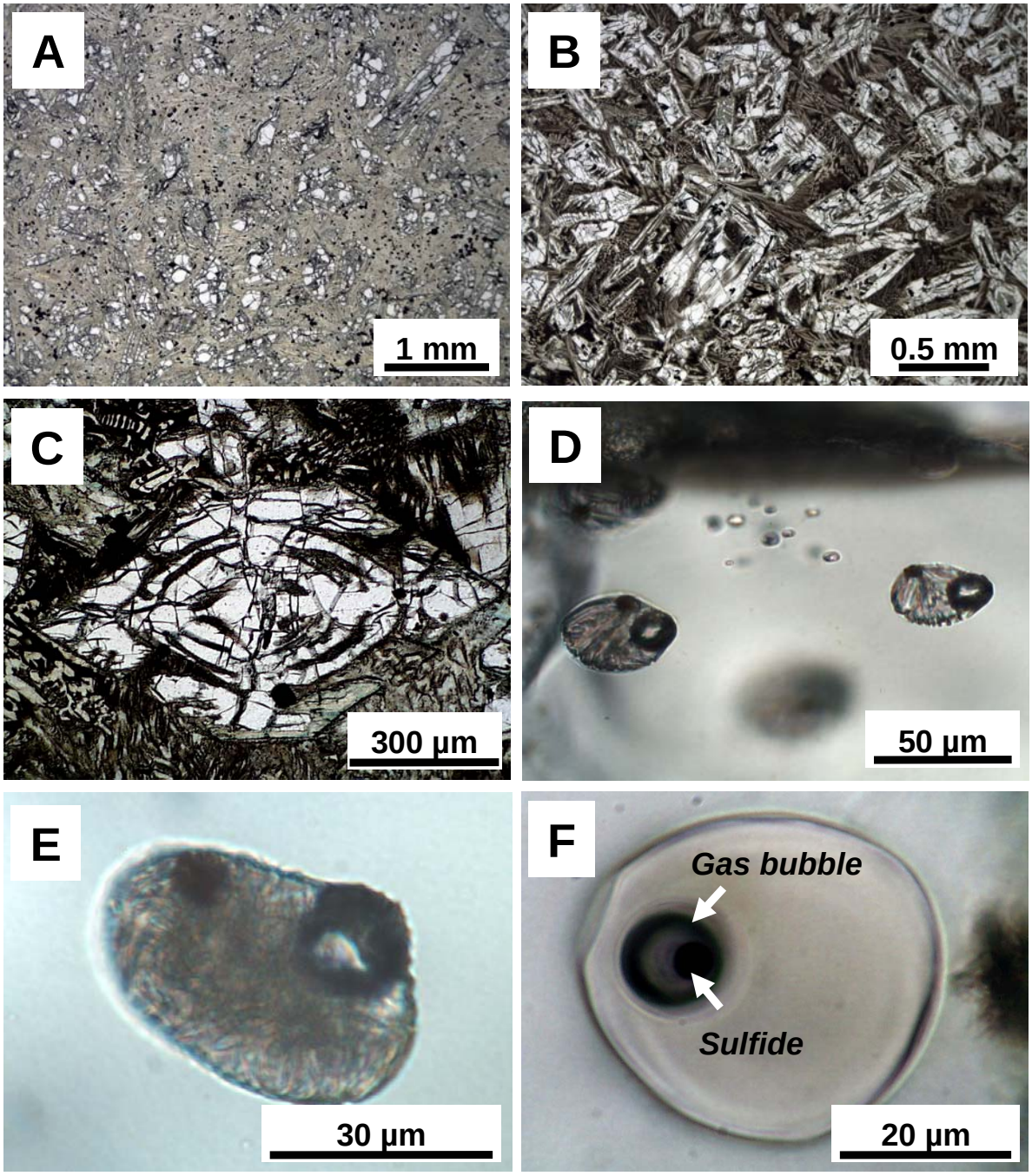

Fig. S1. Photomicrographs showing typical texture of the studied rock samples, the morphology of host olivine and melt inclusions from the Gorgona komatiites. (A) Cumulative zone of the komatiite flow, sample GOR94-44. (B) Joint top flow, sample GOR94-28. (C) Fractured, euhedral olivine crystal from cumulative picrite. (D, E) Unheated, crystallized melt inclusions in olivine. (F) Melt inclusion after re-heating run composed of brownish glass, gas bubble and sulfide globule adhered to the bubble.

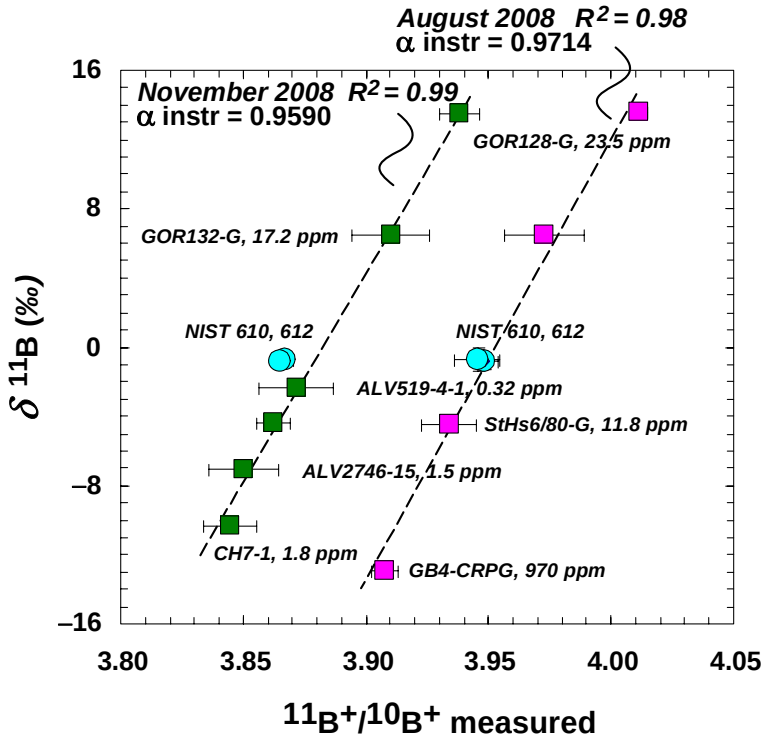

Fig. S2. Boron isotope working curves obtained using a set of natural reference glasses and given in comparison with artificial NIST SRM 610 and 612 standard glasses. Analyses have been done during two analytical sessions in August and November 2008. Bars represent ±2σ SE analytical precision obtained during multiple measurements on the respective reference glass. Depending on the α_{IMF} value, the ~1–2‰ offset between the artificial NIST SRM and natural reference glasses, similar as reported by Rosner et al. (2008), can be recognized during the November 2008 analytical session. This effect can be eliminated when the transmission of the instrument is optimized by reaching the higher α_{IMF} value (0.971 obtained in August 2008 vs. 0.959 in November 2008).

References

Chaussidon, M., Jambon, A., 1994. Boron content and isotopic composition of oceanic basalts: geochemical and cosmochemical implications. Earth Planet. Sci. Lett. 121, 277–291.

Chaussidon, M., Robert, F., Mangin, D., Hanon, P., Rose, E., 1997. Analytical procedures for the measurement of boron isotope compositions by ion microprobe in meteorites and mantle rocks. Geostandards Newsletter, Journal of Geostandards and Geoanalysis 21, 7–17.

Danyushevsky, L.V., McNeill, A.W., Sobolev, A.V., 2002. Experimental and petrological studies of melt inclusions in phenocrysts from mantle-derived magmas: an overview of techniques, advantages and complications: Chem. Geol. 183, 5–24.

Jochum, K.P., Dingwell, D.B., Rocholl, A., et al., 2000. The preparation and preliminary characterization of eight geological MPI-DING reference glasses for in-situ microanalysis. J. Geostand. Geoanalys. 24, 87–133.

Kamenetsky, V.S., Gurenko, A.A., Kerr, A.C., 2010. Composition and temperature of komatiite melts from Gorgona Island constrained from olivine-hosted melt inclusions. Geology 38, 1003–1006.

Kita, N.T., Ushikubo, T, Fu, B., Valley, J.W., 2009. High precision SIMS oxygen isotope analysis and the effect of sample topography. Chem. Geol. 264, 43–57.

Portnyagin, M., Almeev, R., Matveev, S., Holtz, F. 2008. Experimental evidence for rapid water exchange between melt inclusions in olivine and host magma. Earth Planet. Sci. Lett. 272, 541–552.

Rosner, M., Meixner, A., 2004. Boron isotopic composition and concentration of ten geological reference materials. Geostand, Geoanalyt. Res. 28, 431–441.

Rosner, M., Wiedenbeck, M., Ludwig, T., 2008. Composition-induced variations in SIMS instrumental mass fractionation during boron isotope ratio measurements of silicate glasses. Geostand. Geoanal. Res. 32, 27–38.

Sobolev, A.V., Slutskii, A.B., 1984. Composition and crystallization conditions of the initial melt of the Siberian meimechites in relation to the general problem of ultrabasic magmas. Soviet Geol. Geophys. 25, 93–104.

Sobolev AV, Danyushevsky LV (1994) Petrology and geochemistry of boninites from the North Termination of the Tonga Trench: Constraints on the generation conditions of primary high-Ca boninite magmas. J Petrol 35: 1183-1211.

Spivack, A.J., Edmond, J.M., 1986. Determination of boron isotope ratios by thermal ionization mass spectrometry of the dicesium metaborate cation. Anal. Chem. 58, 31–35.